3-1-2021

Extracellular vesicles derived from bone marrow mesenchymal stem cells enhance myelin maintenance after cortical injury in aged rhesus monkeys

Veronica Go

Deniz Sarikaya

Yuxin Zhou

Bethany G.E. Bowley

Monica A. Pessina

See next page for additional authors

Authors

Veronica Go, Deniz Sarikaya, Yuxin Zhou, Bethany G.E. Bowley, Monica A. Pessina, Douglas L. Rosene, Zhenggang Zhang, Michael Chopp, Seth P. Finklestein, Maria Medalla, Benjamin Buller, and Tara L. Moore

Experimental Neurology 337 (2021) 113540

Contents lists available at ScienceDirect

Experimental Neurology

journal homepage: www.elsevier.com/locate/yexnr

Research paper

Extracellular vesicles derived from bone marrow mesenchymal stem cells enhance myelin maintenance after cortical injury in aged rhesus monkeys

Veronica Go [a,*], Deniz Sarikaya [b], Yuxin Zhou [c], Bethany G.E. Bowley [c], Monica A. Pessina [c], Douglas L. Rosene [c,f,i], Zheng Gang Zhang [d], Michael Chopp [d,e], Seth P. Finklestein [g,h], Maria Medalla [c,i], Benjamin Buller [d,1], Tara L. Moore [c,i,1]

[a] Department of Pharmacology & Experimental Therapeutics, Boston University School of Medicine, United States
[b] Research Center for Translational Medicine, Koç University School of Medicine, Turkey
[c] Department of Anatomy & Neurobiology, Boston University School of Medicine, United States
[d] Department of Neurology, Henry Ford Health Systems, United States
[e] Department of Physics, Oakland University, United States
[f] Yerkes National Primate Research Center, Emory University, United States
[g] Department of Neurology, Massachusetts General Hospital, United States
[h] Stemetix, Inc., United States
[i] Center for Systems Neuroscience, Boston University, United States

ARTICLE INFO

Keywords:
Extracellular vesicles
Myelin
White matter
Oligodendrocytes
Non-human primates
Cortical injury
Stroke
Aging
Monkeys

ABSTRACT

Cortical injury, such as stroke, causes neurotoxic cascades that lead to rapid death and/or damage to neurons and glia. Axonal and myelin damage in particular, are critical factors that lead to neuronal dysfunction and impair recovery of function after injury. These factors can be exacerbated in the aged brain where white matter damage is prevalent. Therapies that can ameliorate myelin damage and promote repair by targeting oligodendroglia, the cells that produce and maintain myelin, may facilitate recovery after injury, especially in the aged brain where these processes are already compromised. We previously reported that a novel therapeutic, Mesenchymal Stem Cell derived extracellular vesicles (MSC-EVs), administered intravenously at both 24 h and 14 days after cortical injury, reduced microgliosis (Go et al. 2019), reduced neuronal pathology (Medalla et al. 2020), and improved motor recovery (Moore et al. 2019) in aged female rhesus monkeys. Here, we evaluated the effect of MSC-EV treatment on changes in oligodendrocyte maturation and associated myelin markers in the sublesional white matter using immunohistochemistry, confocal microscopy, stereology, qRT-PCR, and ELISA. Compared to vehicle control monkeys, EV-treated monkeys showed a reduction in the density of damaged oligodendrocytes. Further, EV-treatment was associated with enhanced myelin maintenance, evidenced by upregulation of myelin-related genes and increases in actively myelinating oligodendrocytes in sublesional white matter. These changes in myelination correlate with the rate of motor recovery, suggesting that improved myelin maintenance facilitates this recovery. Overall, our results suggest that EVs act on oligodendrocytes to support myelination and improves functional recovery after injury in the aged brain.

Significance: We previously reported that EVs facilitate recovery of function after cortical injury in the aged monkey brain, while also reducing neuronal pathology (Medalla et al. 2020) and microgliosis (Go et al. 2019). However, the effect of injury and EVs on oligodendrocytes and myelination has not been characterized in the primate brain (Dewar et al. 1999; Sozmen et al. 2012; Zhang et al. 2013). In the present study, we assessed changes in myelination after cortical injury in aged monkeys. Our results show, for the first time, that MSC-EVs support recovery of function after cortical injury by enhancing myelin maintenance in the aged primate brain.

Abbreviations: EVs, extracellular vesicles; MSC, Mesenchymal Stem Cells; SW, sublesional white matter; OPCs, oligodendrocyte precursor cells; MBP, Myelin Basic Protein.

* Corresponding author at: 700 Albany Street, W701, Boston, MA 02118, United States.
E-mail address: vgo@bu.edu (V. Go).

[1] These authors share senior authorship.

https://doi.org/10.1016/j.expneurol.2020.113540
Received 26 April 2020; Received in revised form 5 November 2020; Accepted 24 November 2020
Available online 29 November 2020

1. Introduction

Cortical injury, such as stroke or age-related pathology, causes rapid apoptosis and necrosis of neurons and glia. Damage to axons and myelin, in particular, are crucial factors that contribute to neuronal dysfunction and is often exacerbated in the aged brain where white matter damage is prevalent. Oligodendrocytes, cells that produce and maintain myelin, facilitate neuronal function in the Central Nervous System (CNS). Specifically, oligodendrocytes support neurons by providing axonal stability, maintaining axonal metabolism, and improving axonal conduction. While oligodendrocytes are critical for normal neuronal function, they are extremely susceptible to cytotoxic and inflammatory damage associated with neurotraumatic injuries - especially in the aged brain - due to the release of cytotoxic proteases, inflammatory cytokines, and reactive oxygen species (Arai and Lo 2009; Chavez et al. 2009; Lakhan et al. 2009; Wang et al. 2016). These cytotoxic agents produce lasting damage to oligodendrocytes, in addition to neurons and other glial cells, thus causing injury to cells necessary to support neurological functions (Wang et al. 2007; Arai and Lo 2009). With such impairments in oligodendrocytes, neurons become increasingly susceptible to structural and functional disturbances (Wang et al. 2007; Chavez et al. 2009)and, resulting in sustained neuronal dysfunction (Duncan et al. 1997; Wang et al. 2016).

Myelin pathology and oligodendrocyte dysfunction are prevalent in the aged brain and likely contribute to age-related susceptibility to brain injury and subsequent neuronal dysfunction (Bowley et al. 2010; Shobin et al. 2017). In particular, oligodendrocytes found in the aged brain are more susceptible to increased levels of degrading enzymes such as calpain (Sloane et al. 2003) as well as increased levels of oxidative damage to oligodendroglial DNA (Tse and Herrup 2017). Additionally, oligodendroglia have reduced proliferative and differentiation capabilities with increased age, thus dampening their ability to restore myelin (Miyamoto et al. 2013; El Waly et al. 2014; Rivera et al. 2016). In essence, increased susceptibility to damage and degradation of oligodendrocytes, as well as reduced oligodendrogenesis associated with age, results in decreased myelination and oligodendrocyte function which can contribute to reduced neurological function. Hence, limiting the extent of oligodendrocyte damage and facilitating oligodendrocyte proliferation and maturation could enhance myelin maintenance and promote neurorestoration in aged, injured, and diseased brains (Arai and Lo 2009; Takase et al. 2018). Therefore, therapeutic agents that facilitate myelin maintenance may improve neurological outcomes following injury, especially in the aged brain.

One promising novel therapy is extracellular vesicles (EVs) derived from bone marrow Mesenchymal Stem Cells (MSCs), which have been shown to produce regenerative effects for brain injury and neurodegeneration *via* restorative processes such as immunomodulation, angiogenesis, neurogenesis, and synaptogenesis both *in vivo* and *in vitro* in rodent, porcine, and primate models (Chopp and Li 2002; Zhang et al. 2019; Moore et al., 2019). While cell-based therapies, including MSCs, have been useful for restorative therapy, the mechanism is likely through the release of EVs, which are nano-scale vesicles that contain miRNA, mRNA, and protein that are crucial for intercellular communication (Xin et al. 2012). These EVs are taken up by a recipient cell, which putatively responds to the molecular content delivered by the EVs. Currently, the effects of EV therapy on oligodendrocytes and myelin *in vivo* are largely unknown, especially in the aged primate brain.

Our previous work has tested EVs as a therapeutic for brain injury in rodent and porcine models (Chopp and Li 2002; Zhang et al. 2019). Most recently, we tested the therapeutic potential of MSC-EVs for enhancing motor recovery following cortical injury in the hand representation of the primary motor cortex of aged monkeys (Moore et al. 2019). Aged monkeys treated with MSC-EVs recovered fine motor function of the hand and digits within 3–5 weeks compared to aged monkeys in the vehicle control group (PBS) which exhibited a more limited recovery (Moore et al. 2019). Further, we have shown that EV treatment reduces microgliosis (Go et al. 2019) and neuronal pathology (Medalla et al. 2020) in the aged brain, which could partially explain the enhancement of motor recovery described in (Moore et al. 2019). However, the downstream effects of EVs on myelin remains unclear. In the present study, we used archived tissue from the same aged brains studied in Moore et al. (2019) and assessed myelination with and without EV treatment after cortical injury. To our knowledge, this is the first study to assess the effects of MSC-EVs on myelination after cortical injury in aged rhesus monkeys.

2. Methods

2.1. Subjects

Brain tissue used in this study was from nine aged female rhesus monkeys used in Moore et al. 2019. The monkeys ranged in age from 16 to 26 years old (analogous to humans approximately 48 to 78 years old, Tigges et al. 1988, Supplementary Table 1). Monkeys were acquired from national research primate centers and private vendors, and were maintained in the Animal Science Center of Boston University Medical Campus (fully AAALAC accredited). Experiments were approved by the Boston University Institutional Animal Care and Use Committee. During the study, aged monkeys were individually housed within visual and auditory range of other monkeys in the colony room. Enrichment procedures used either met or exceeded USDA requirements. Aged monkeys were fed once a day, immediately following testing, and water was available continuously. Diet consisted of a commercial monkey chow that was supplemented with fruits and vegetables. Before entering the study, monkeys were assessed for pre-existing abnormalities in overall health. As detailed in Moore et al. (2019), monkeys were trained on a fine motor task then randomly assigned to a vehicle control or EV treatment before receiving a cortical injury targeted to the hand representation of the primary motor cortex (M1). Following injury, they were given intravenous vehicle control (PBS) or EV treatment (4×10^{11} particles/kg) at 24 h after surgery and again at 14 days after surgery. All staff were blinded to the treatment groups for all procedures and experiments.

2.2. Mesenchymal stem cell-derived extracellular vesicle preparation and administration

EVs were isolated from bone marrow derived MSCs of a young monkey, as described previously (Xin et al. 2013; Moore et al. 2019). Briefly, a young monkey (approximately 5 years old - equivalent to 15 human years) was sedated with ketamine (10 mg/kg IM), then anesthetized with sodium pentobarbital (15–25 mg/kg IV). Bone marrow was extracted from the iliac crest and shipped on wet ice, with same day delivery to Henry Ford Health Systems in Detroit. Upon arrival, marrow was spun at 4000 x*g* for 15 min to separate cells. The buffy coat was discarded, and remaining cells were washed in culture medium. Cells were then plated in a T75 flask using media containing 20% FBS and alpha-MEM, grown to confluence, and passaged as necessary. To grow enough cells for EVs, 10×10^6 cells were seeded into a Quantum Incubator (Terumo BCT, Lakewood, CO) and grown in alpha-MEM with 10% EV-depleted FBS (Systems Biosciences, Palo Alto, CA). To harvest EVs, media was collected every other day for four days, then every day for two days. As described in Zhang et al. (2015), media was centrifuged in multiple stages at 250 x*g* for 5 min, then 3000 x*g* for 30 min, then filtered and centrifuged a final time at 100,000 x*g* for 2 h to pellet EVs. The pellet was resuspended in a small volume of PBS. EV concentrations and particle sizes were measured using a qNano (Izon, Cambridge, MA, United States), then diluted to 4×10^{11} particles/kg for each monkey in 4 mL of PBS. EVs had an average diameter of 111 nm in size (Supplementary Fig. 1), and had confirmed expression of CD9, CD81, and CD63 by western blot, per MISEV guidelines (data not shown) (Witwer et al. 2017). The dose was chosen based on previous dosing studies conducted

in rats (Xin et al. 2013; Zhang et al. 2015). Following resuspension, EVs were stored at 4 °C until the day before treatment, then shipped to Boston University the day prior to intravenous administration in monkeys.

2.3. Motor testing and lesion of the M1 hand representation

To assess motor function, monkeys were trained on the Hand Dexterity Task (HDT) for five weeks, a modified version of the Klüver board, as described in (Moore et al. 2012, 2013, 2019). After pre-training, the dominant hand was determined using free choice trials. To create an injury in the hand representation of M1, a craniotomy was performed over the contralateral hemisphere of the dominant hand. The dura was opened, and the precentral gyrus was electrophysiologically mapped using a small silver ball surface electrode to locate the precise area of M1 that controlled hand and digit function. Using this map, a small incision was made in pia above the hand representation, and a small glass suction pipette was placed under the pia to bluntly separate penetrating arterioles from the underlying cortex in the mapped area as well as through the adjacent anterior bank of the central sulcus. This approach disrupts the blood supply to the underlying cortex without mechanically damaging the underlying grey matter. After injury, monkeys were given two weeks to recover, then monkeys resumed fine motor testing for 12 weeks to assess the rate and extent of recovery of fine motor function on the HDT, with and without EV treatment.

2.4. Cerebrospinal fluid extraction

Cerebrospinal fluid (CSF) was drawn at multiple time points across the recovery period (Baseline (Pre-surgery), 14 days after injury, 28 days after injury, 6 weeks after injury, and at euthanasia 14 weeks after injury) to assess Myelin Basic Protein. Briefly, monkeys were sedated with Ketamine (10 mg/kg IM), CSF was drawn from the cisterna magna and immediately placed in 4 °C for temporary storage (less than 2 h), then frozen and stored at −80 °C until processed.

2.5. Brain tissue section preparation and storage

Following completion of motor testing (Moore et al. 2012, 2013, 2019) monkeys were sedated with ketamine (10 mg/kg IM) and anesthetized with intravenous sodium pentobarbital (25 mg/kg IV to effect). While under a surgical level of anesthesia, the chest was opened and monkeys were euthanized by exsanguination during transcardial perfusion-fixation of the brain, first with cold Krebs-Heinsleit buffer (4 °C, pH 7.4) during which fresh tissue biopsies were collected, after which the perfusate was switched to 4% paraformaldehyde (30 °C, pH 7.4) to fix the brain. Fresh tissue was immediately snap frozen in pulverized dry ice, then stored at −80 °C until processed.

The fixed brains were blocked, *in situ*, in the coronal plane, removed from the skull, and cryoprotected in a solution of 0.1 M phosphate buffer, 10% glycerol, and 2% DMSO followed by buffer with 2% DMSO and 20% glycerol. Brains were then flash frozen at −75 °C in isopentane and stored at −80 °C (Rosene et al., 1986). For histological analyses, brains were removed from the −80 °C storage and cut on a microtome in the coronal plane into interrupted series (8 series of 30 μm sections, and one 60 μm section series) giving a 300 μm spacing between sections in each series. If not processed immediately, sections were transferred to cryoprotectant (15% glycerol in buffer) and stored at −80 °C until thawed for immunohistochemistry.

2.6. Regions of interest

Sections containing the lesion were first identified in a series of thionin stained coronal sections from each monkey based on the presence of tissue damage in the hand area of primary motor cortex, indicated by glial scarring, disrupted neuronal profiles, and discontinuity of the pial surface and cortical lamination, as described previously (Orczykowski et al., 2018). Within the range of sections containing the lesion, a subset of sections spaced 2400 μm apart was selected for further analysis with defined the regions of interest (ROI) which included the sublesional white matter (SW) - delineated as the white matter immediately beneath the grey matter lesion. Coronal sections from adjacent series were matched to thionin-stained sections containing the lesion and selected for immunofluorescent labeling of markers (Fig. 1A). To illustrate the typical distribution of oligodendrocytes in a normal, aged brain, images from the white matter from the contralateral primary motor cortex were scanned and denoted as “controls”, as shown in Figs. 2, 4, and 5.

2.7. Fluorescent immunohistochemistry of oligodendroglial markers

Three tissue sections through the lesion, spaced 2400 μm apart (selected based on the thionin series), were removed from −80 °C, thawed, and batch processed with immunohistochemistry to assess oligodendroglial markers. Sections were washed with PBS, blocked using Superblock (ThermoFisher, Waltham, MA, USA), then incubated overnight at RT with primary antibodies (single, double, or triple-labeled) to rabbit anti-BCAS1 (marker of newly myelinating oligodendrocytes, Abcam, ab106661, Fard et al. 2017), mouse anti-CC1 (marker of mature oligodendrocytes, Abcam, ab16794), rabbit anti-Olig2 (marker of all oligodendrocyte lineage, Abcam, ab42453), mouse anti-8OHdG (marker of oxidative DNA damage, Abcam, ab62623), and rabbit anti-NG2 (marker of Oligodendrocyte Precursor Cells, Abcam, ab129051) in a PBS solution containing 0.5% Superblock and 0.3% Triton-X (Supplementary Table 2). Following an overnight incubation, tissue was washed, then incubated in the appropriate fluorescent secondary antibodies (goat anti-rabbit, goat anti-mouse at 1:200, Supplementary Table 2) in a PBS solution containing 0.5% Superblock and 0.3% Triton-X. Tissue was washed again, then counterstained with DAPI (1:1000) in PBS for 30 min RT. Sections were then placed in cupric sulfate for 15 min at RT to reduce autofluorescence (Schnell et al. 1999) and rinsed briefly in dH_2O. Finally, sections were mounted, air-dried for 30 min, coverslipped in DABCO mounting medium (Sigma Aldrich, St. Louis, MO, USA), and stored at −20 °C until ready to be imaged.

2.8. Confocal imaging of oligodendroglial cells

Fluorescently labeled oligodendroglia were imaged with a Leica TCS SPE laser scanning confocal microscope, using UV, 488 and 561 diode lasers. To ensure proper blinding, slides were blinded by assigning codes prior to imaging. For each section, 12 images were taken through the SW, spaced 500 μm apart. Each site was imaged through the z-stack using a 40 × 1.3 N.A. oil objective lens at a resolution of 0.135 × 0.135 × 1.0 μm per voxel. Confocal *Z*-stack images were deconvolved, and converted to 8-bit images using AutoQuant (Media Cybernetics) to improve the signal-to-noise ratio, as described (Medalla and Luebke 2015).

2.9. Spectral confocal reflectance microscopy imaging

Spectral Confocal Reflectance (SCoRe) Microscopy as described in (Schain et al. 2014; Hill et al. 2018) was used to assess the density of myelinated axons at the junction of perilesional grey matter and sublesional white matter (Layer VI). Briefly, 30 μm sections were mounted onto gelatin-subbed slides, air-dried for 30 min, then coverslipped using prolong gold (ThermoFisher, Waltham, MA, USA). Slides were imaged on a Leica TCS SPE laser scanning confocal microscope using a 40 × 1.3 numerical aperture oil immersion objective by exciting slides with 488, 561, and 647 laser diodes. Slides were imaged at a resolution of 0.135 × 0.135 × 1.0 μm per voxel through the z-stack in four regions of Layer VI spaced 500 μm apart.

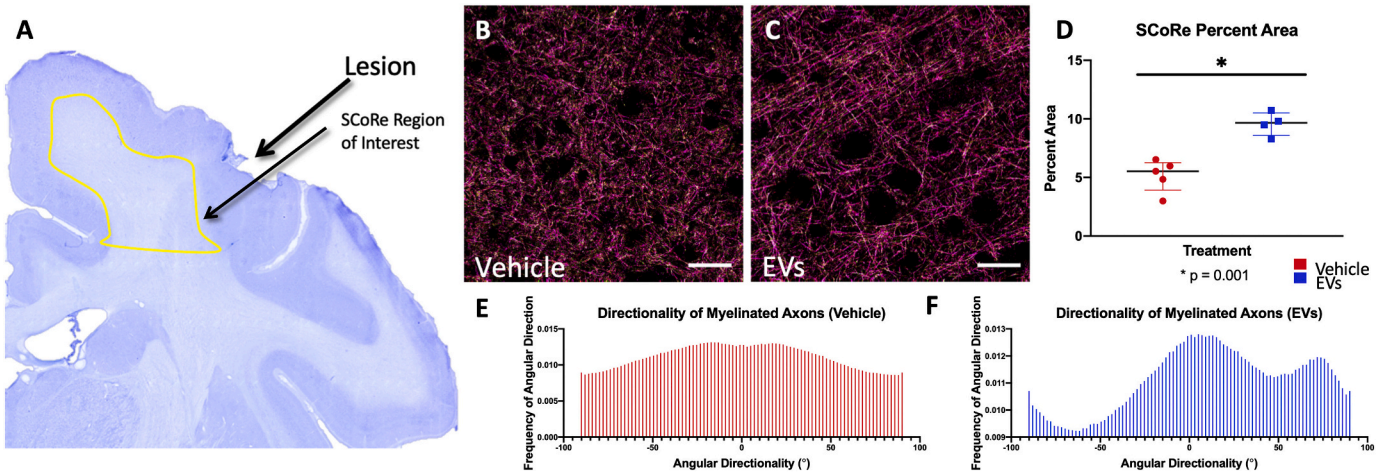

Fig. 1. Spectral Confocal Reflectance (SCoRe) Microscopy demonstrates increased densities of myelinated axons in the EV group as well as more defined fiber orientations. A) Regions of interest for Spectral Confocal Reflectance Microscopy were aligned beneath the lesion, adjacent to the junction of Layer VI. B&C) Representative images of myelinated axons in Layer VI of the perilesional grey matter. D) Image analysis of SCoRe images revealed a greater density of myelinated axons in the EV group ($p = 0.001$). E&F) Assessment of the directionality and orientation of the myelinated axons revealed different distributions (Kolmogorov-Smirnov test p = 0.04) between Vehicle (E) and EV groups (F). Directionality analyses demonstrated fibers in vehicle treated brains had a relatively uniform orientation, confirming the appearance in (B). In contrast, (F) shows axons in the EV group with a bimodal distribution of axon orientation, indicating a more linear, grid-like organization (C). Scale bar = 50 μm.

2.10. Quantification and analysis of oligodendroglia

All images were analyzed using ImageJ. To assess densities of BCAS1+ (new myelinating cells) and CC1+ (mature oligodendrocytes) cells, 8OHdG+ (oxidative DNA damage marker) and Olig2+ (general oligodendrocyte marker) cells, and NG2+ oligodendrocyte precursor cells, images were opened, channels were split, then merged again to create a composite image. To estimate oligodendrocyte cell densities, cells were counted through the z-stack using the plugin "Cell Counter" (https://imagej.nih.gov/ij/plugins/cell-counter.html), a plugin that allows for manual counting by marking each cell with a marker using adapted stereological rules (Fiala and Harris 2001). To analyze oligodendrocytes with and without oxidative DNA damage, blinded double-labeled images of 8OHdG+ and Olig2+ cells were separated into oligodendrocytes with (Olig2+/8OHdG+) and without oxidative DNA damage (Olig2+/8OHdG-). Similarly, slides single-labeled for oligodendrocyte precursor cells positive for NG2 immuno-reactivity were analyzed using the cell counter to estimate cell densities.

To quantify BCAS1+ cells, labeled cells were stratified based on morphology and BCAS1+ expression levels. Since BCAS1 is transiently expressed during oligodendrocyte maturation, oligodendrocytes were separated into distinct maturation stages. Briefly, as described in Fard et al. (2017), oligodendrocyte precursor cells (OPCs) first express BCAS1 only in the soma (BCAS1+/CC1-). As they mature, they express BCAS1+ more strongly in both the soma and in long, radiating processes (30 μm or longer; BCAS1++/CC1-). Eventually, CC1, a marker of mature oligodendrocytes is expressed in the soma where it colocalizes with BCAS1+ cells (BCAS1++/CC1+). Finally, expression of BCAS1+ begins to decrease in the processes, but remains in the soma colocalized with CC1+, indicating maturation of OPCs into mature oligodendrocytes (BCAS1+/CC1+). Next, in the last stage of maturation, BCAS1+ expression ceases, and CC1+ alone is expressed (Fard et al., 2017). Thus, for the quantification of oligodendrocytes, with and without BCAS1+ and CC1+ staining, we stratified oligodendrocytes into five distinct maturation stages: BCAS1+/CC1-, BCAS1++/CC1-, BCAS1++/CC1+, BCAS1+/CC1+, and CC1.

SCoRe images were analyzed using particle analysis on ImageJ by thresholding and assessing the percent area containing reflectance from myelinated axons. Additionally, we assessed the directionality and orientation of the myelinated fibers using the ImageJ plugin "directionality" (https://imagej.net/Directionality), a plugin that assigns angular direction to individual fibers and determines the frequency of each angular orientation.

2.11. Enzyme-linked immunosorbent assay myelin basic protein

To assess myelin damage, we used an Enzyme Linked Immunosorbent Assay (ELISA; Ansh Labs, Houston, TX, USA) to measure longitudinal levels of Myelin Basic Protein (MBP) in CSF. Previous literature has demonstrated that MBP is found in CSF of patients when a demyelinating lesion is present (Ohta and Ohta 2002). The ELISA was performed according to the manufacturer's protocol. Briefly, CSF samples from every time point (pre-operative, 14 days, 28 days, 6 wks, and 14 wks after injury) across all animals were thawed at the same time and diluted 1:2 using assay buffer. Standards were reconstituted according to the manufacturer's protocol and standards and samples were plated in duplicate. Samples were gently agitated on an orbital shaker at 800 RPM for one hour, then decanted and washed. Samples were then incubated in anti-MBP antibody and agitated at 800 RPM for one hour at RT on an orbital shaker. Solution was decanted, the plate was washed, and a biotinylated conjugate was added, then incubated and agitated for 30 min at RT at 800 RPM. Solution was decanted again, and the plate was washed. Finally, a chromogen detection solution was added and incubated for 20 min in the dark on the orbital shaker and read immediately on a plate reader (BioRad, Berkeley, California, USA).

2.12. RNA isolation and qPCR of myelin related genes

Fresh-frozen perilesional brain tissue containing white matter dissected at euthanasia (14 wks after injury) from all animals was used for this study. Tissue samples were removed from −80 °C storage, placed on dry ice, then dissected into 100 mg pieces (one for each animal). Each sample was mechanically homogenized using an RNAse free scalpel, then chemically triturated using the TRIzol method (ThermoFisher, Waltham, MA). Briefly, tissue was placed in TRIzol, then passed through an 18-gauge needle to further homogenize tissue. An organic extraction was then performed using chloroform and ethanol, according to the manufacturer's protocol (ThermoFisher, Waltham, MA). The extracted RNA was then air-dried, resuspended in 40 μL of PCR-grade water, then checked for A260/280 using a NanoDrop (ThermoFisher, Waltham,

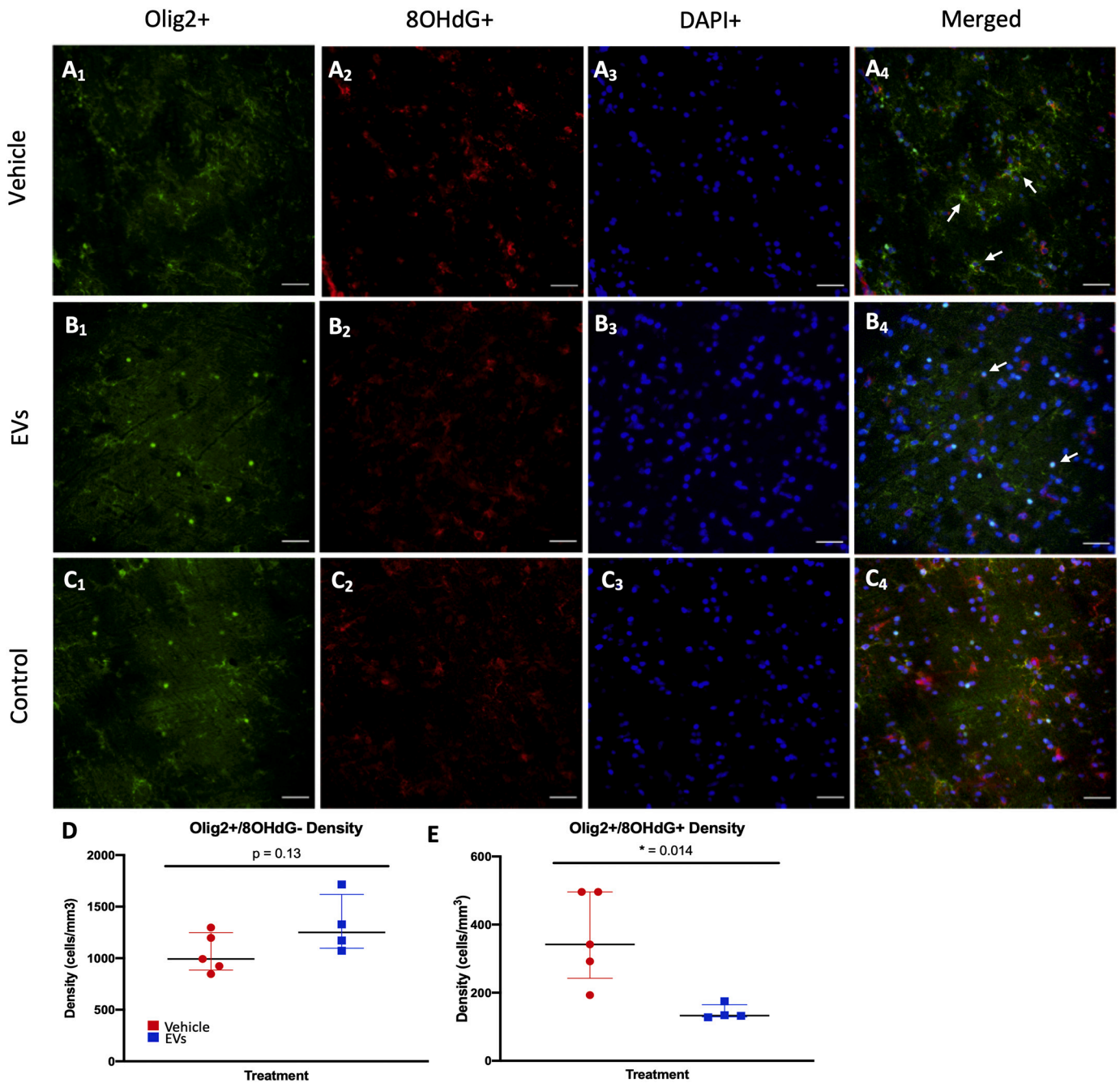

Fig. 2. Densities of oligodendrocytes (Olig2) colocalized with 8OHdG, a marker of oxidative DNA damage, showed reduced oxidative damage to oligodendrocytes in EV-treated monkeys. Tissue sections stained with Olig2, 8OHdG, and DAPI counterstaining were imaged with confocal microscopy in the sublesional white matter. A_1, B_1, and C_1) Oligodendrocytes labeled with Olig2 (general oligodendrocyte marker). A_2, B_2, and C_2) Sections labeled with 8OHdG (oxidative DNA damage). A_3, B_3, and C_3) DAPI counterstaining was used to label nuclei. A_4, B_4, and C_4) Merged images of oligodendrocytes stained with 8OHdG, Olig2, and DAPI counterstaining represent oligodendrocytes with oxidative DNA damage present. $C_1 - C_4$) Representative images of Olig2+ and 8OHdG+ labeling in the contralateral white matter of the motor cortex illustrates the typical distribution of Olig2 and 8OHdG labeling in a non-lesioned monkey. D) There were no statistically significant differences in the densities of Olig2+ oligodendrocytes without DNA damage in the EV-treated animals ($p = 0.13$). E) Cell density analysis of Olig2+ oligodendrocytes, co-labeled with 8OHdG (DNA damage marker), revealed reduced densities of oligodendrocytes with DNA-damage in the EV-treated animals ($p = 0.014$). Arrows mark cells co-labeled with Olig2+ and 8OHdG+ staining. Scale bar = 50 μm.

MA).

Following extraction, RNA was converted to cDNA using a High Capacity RNA-to-cDNA kit (ThermoFisher, Waltham, MA), according to the manufacturer's protocol, then normalized to 2 μg for each sample. Finally, qPCR was performed in triplicate using forward and reverse kiqStart primers (Sigma Adlrich, St. Louis, MO) for Myelin Basic Protein (MBP), a marker of mature myelinating oligodendrocytes; Myelin Regulatory Factor (MyRF), a gene for oligodendrocyte differentiation and regulation; Breast Carcinoma Amplified Sequence 1 (BCAS1), a gene upregulated in new myelinating oligodendrocytes; and GAPDH as a housekeeping gene.

2.13. Data analysis and statistics

All of the studies were performed with the experimenter blinded to treatment groups. To assess any treatment specific group differences,

SCoRe signal and cell density counts were all analyzed using unpaired two-sample Student's *t*-tests. To further assess the axons (imaged by SCoRe), we assessed histogram outputs from the directionality plugin and used the Kolmogorov-Smirnov test to assess differences in the distribution of myelinated axon orientation. To evaluate longitudinal measures of Myelin Basic Protein in CSF, a two-way ANOVA was performed to assess any differences between groups or time points. To assess relative fold changes of myelin gene expression of the EV group relative to the vehicle control group at 14 weeks post-injury, we used the ddCT analysis method. Finally, to assess relationships between myelin measurements and recovery, we used Pearson's correlation. Due to the availability of using only female subjects in the study, we did not evaluate the effect of sex as a variable in any analysis. All tests were analyzed using an alpha of $p \leq 0.05$ to determine significance.

2.14. Data availability

The data that support the findings in this study are available from the corresponding author upon request.

3. Results

3.1. Density and organization of myelinated axons

We used Spectral Confocal Reflectance (SCoRe) microscopy to assess the density and orientation of myelinated axons in the superficial white matter, adjacent to the junction of cortical layer VI within the sublesional area (Fig. 1A). SCoRe is a label-free method to image myelin reflectance on axons (Fig. 1B&C), thereby visualizing only axons that are myelinated (Schain et al. 2014; Hill et al. 2018). Myelin surrounding axons that have undergone damage often fragments and becomes granular, isotropic, and less organized as the fibers breakdown into fragments of myelin debris (Alizadeh et al. 2015). We found that the EV-treated group had a significantly greater percent area of SCoRe positive (SCoRe+) myelinated axons than the vehicle control group ($t(7) = 5.061$, $p = 0.014$, Fig. 1D). Additionally, analyses of the distribution of myelinated axon orientation revealed a difference between groups (Kolmogorov-Smirnov test, $D = 0.211$, $p = 0.04$, Fig. 1E&F). Specifically, the EV group showed a bimodal distribution of myelinated fiber orientation (Fig. 1C&F), while the vehicle control group showed a uniform distribution, with no clear peak, suggesting a lack of organization of the myelinated fibers (Fig. 1B&E). Indeed, SCoRe+ axons in the superficial sublesional white matter exhibited a grid-like appearance in EV brains (Fig. 1C), while SCoRe + axons in vehicle brains had randomized orientations (Fig. 1B). These data suggest that EV brains have greater densities and organization of SCoRe+ axons, which reflects more intact myelin with EV treatment after injury (Fig. 1B&C).

3.2. EV treatment decreases the density of oligodendrocytes with oxidative damage

We then assessed whether EV treatment affected injury-related damage of oligodendrocytes by quantifying the densities of oligodendrocytes (Olig2) with and without co-labeling of 8OHdG, a marker of oxidative DNA damage (Fig. 2A_1–C_4). When we assessed the density of oligodendrocytes without oxidative DNA damage (Olig2+/8OHdG-), we found no statistically significant differences between groups ($t(7) = 1.723$, $p = 0.13$, Fig. 2D). However, the density of oligodendrocytes with oxidative DNA damage (Olig2+/8OHdG+) was lower in the EV-treated group ($t(7) = 3.275$, $p = 0.014$, Fig. 2E) compared to the vehicle control group. These data suggest that EV treatment reduced damage to oligodendrocytes.

3.3. Similar levels of myelin basic protein in CSF longitudinally between treatment groups

The greater densities of myelinated axons quantified using SCoRe analysis and the reduction of oligodendrocytes with damaged DNA resulting from EV treatment likely reflect less myelin degeneration but may also be due to increased oligodendrocyte proliferation and maturation enabling myelin maintenance. Thus, we assessed both myelin damage and myelin maintenance using a combination of ELISA, which measured Myelin Basic Protein (MBP) in CSF as a marker of damaged myelin, and qPCR, to assess myelin-related gene expression as a marker of myelin maintenance. Previous literature has demonstrated that high levels of MBP are found in the CSF when there is active demyelination but low to undetectable levels are found when there is no demyelination occurring (Ohta and Ohta 2002). While MBP in CSF is a marker of damage, expression of myelin genes at the transcriptomic level, such as MBP, MyRF, and BCAS1, is considered a marker of oligodendrocyte maturity and myelination, and indicates greater myelin maintenance (Michel et al. 2015).

When we quantified MBP longitudinally in the CSF across the recovery period, there were no statistically significant overall differences between the treatment groups ($F(1,35) = 1.48$, $p = 0.234$, Fig. 3A), time points ($F(4,35) = 1.911$, $p = 0.15$, Fig. 3A), or interaction between group and time points ($F(4,35) = 1.734$, $p = 0.184$, Fig. 3A). However, while these findings were not significant, there appeared to be an increase in MBP levels (at 14 days and at 28 days), as well as increased variability, in the vehicle control animals, followed by a gradual decline longitudinally. In contrast, the EV group demonstrated consistently lower levels of MBP longitudinally with lower variability, suggesting that there may have been less myelin damage in the EV group (Fig. 3A).

3.4. EV treatment increases myelin gene expression relative to the vehicle control

We further assessed potential changes in myelination by performing qRT-PCR on fresh-frozen perilesional tissue to quantify the relative fold change in gene expression of factors related to myelin synthesis and maintenance in the EV group compared to the vehicle control group at 14 weeks after injury. As shown in Fig. 3B, we found a 4-fold increase in Myelin Regulatory Factor, a gene for myelin regulation and oligodendrocyte differentiation, a 1.5-fold increase in Breast Carcinoma Amplified Sequence 1 (BCAS1+), a marker of new myelinating oligodendrocytes, as well as a 1.5-fold increase in the expression of Myelin Basic Protein (MBP), a marker of mature oligodendrocytes (Fig. 3B). Together, these results suggest that the EV-treatment likely enhanced myelination.

3.5. EV treatment increases the density of BCAS1+ and CC1+ oligodendroglia

The extent of oligodendrocyte proliferation and maturation can be indicative of the degree of myelin turnover (Miron et al. 2011; Zhang et al. 2013; Lloyd and Miron 2019). We assessed distinct oligodendrocyte populations expressing markers associated with different stages of maturation and myelination. We quantified the density of the NG2+ oligodendrocyte precursor cells (OPCs) and found no significant differences between treatment groups ($t(7) = 2.408$, $p = 0.08$, Fig. 4D). We then examined potential differences in the densities of differentiated, myelinating oligodendrocytes that were positive for CC1 (a marker of mature myelinating oligodendrocytes) or BCAS1 (a transient marker of new myelinating oligodendrocytes) using stereological counting of individual cell somata. As shown in Fig. 5, we found a significantly greater density of CC1+ cells in EV-treated monkeys compared to vehicle control monkeys ($t(7) = 4.258$, $p = 0.004$, Fig. 5D), indicative of the overall greater density of mature myelinating oligodendrocytes. However, the overall population of BCAS1 labeled cells did not differ between

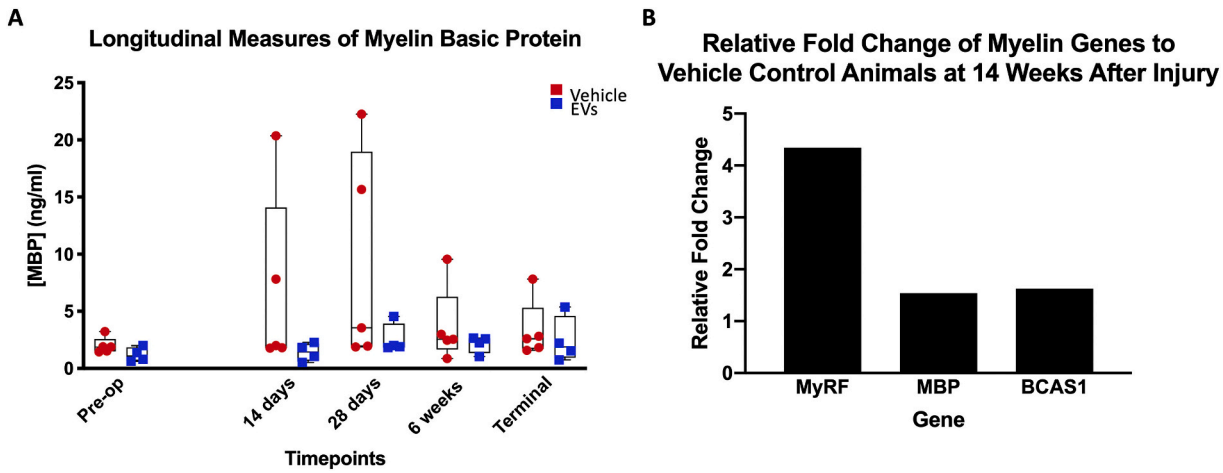

Fig. 3. Longitudinal measures of Myelin Basic Protein (MBP) in cerebrospinal fluid (CSF) and Quantitative Real Time – Polymerase Chain Reaction of myelin related genes in brain tissue 14 weeks after injury. A) An Enzyme-Linked Immunosorbent Assay (ELISA) was used to assess the levels of Myelin Basic Protein in the CSF longitudinally. MBP can be found in the CSF when there is myelin damage present. While EV treatment appeared to reduce a temporal increase in MBP in the CSF in the first 4 weeks after the lesion, there were no statistically significant differences between treatment groups ($F(1,35) = 1.48$, $p = 0.234$), time points ($F(4,35) = 1.911$, $p = 0.15$), or the interaction between group and time points ($F(4,35) = 1.734$, $p = 0.184$) when assessed with ANOVA. The space between "Pre-Op" and "14 days" denotes a gap between the CSF collection timepoints. B) qRT-PCR and the ddCT method were used to quantify fold changes in the EV group relative to the vehicle control group in fresh brain tissue collected at euthanasia, 14 weeks after injury. There was a 4-fold increase in the expression of Myelin Regulatory Factor (MyRF), a gene necessary for oligodendrocyte differentiation, proliferation, and maintenance, a 1.5-fold increase of Myelin Basic Protein (MBP), a gene expressed by mature, myelinating oligodendrocytes, and a similar 1.5-fold increase in Breast Carcinoma Amplified Sequence 1 (BCAS1+), a gene expressed in new myelinating oligodendrocytes.

treatment groups ($t(7) = 1.735$, $p = 0.127$, Fig. 5E).

We then assessed the co-expression of CC1 with BCAS1 to specifically label distinct maturation stages of oligodendrocytes. Previous literature has suggested that the level of BCAS1 expression represents specific stages of myelination (Fard et al. 2017). To assess this, we separated the oligodendrocytes into cells with either low BCAS1 expression (BCAS1+) or high BCAS1 expression (BCAS1++) defined as cells with BCAS1 expressed in both the soma as well as multiple processes (~30 μm or more, Fig. 6A). We then further stratified cells by assessing co-localization with CC1+ (BCAS1+/CC1-, BCAS1++/CC1-, BCAS1++/CC1+, BCAS1+/CC1+). Weakly expressing BCAS1+ cells (BCAS1 expression restricted to the soma), without immunoreactivity for CC1 (BCAS1+/CC1-), are thought to be newly transcribing BCAS1+ and are cells that are converting from a precursor stage towards a myelinating stage. Strongly expressing BCAS1++ cells, with or without co-expression of mature oligodendrocyte markers (BCAS1++/CC1- or BCAS1++/CC1+) are thought to be more mature than BCAS1+/CC1- cells, and are likely to be actively myelinating (Fard et al., 2017). As the oligodendrocyte reaches full maturation, BCAS1 immunoreactivity begins to diminish and processes are no longer immunoreactive for BCAS1+ labeling, defined by a subset of weakly-expressing BCAS1+ (BCAS1+ only in the soma) mature oligodendrocytes with strong CC1 expression (BCAS+/CC1+; Fard et al. 2017, Fig. 6C). When oligodendrocytes were stratified based on maturation stages, compared to the vehicle control group, EV treated brains exhibited a greater density of BCAS1++/CC1- ($t(7) = 2.673$, $p = 0.032$, Fig. 5G) and BCAS1++/CC1+ ($t(7) = 3.242$, $p = 0.014$, Fig. 5H) cells. In contrast, the two groups did not significantly differ with regard to the BCAS1+/CC1- oligodendrocytes ($t(7) = 0.443$, $p = 0.671$, Fig. 5F), nor the BCAS1+/CC1+ cells ($t(7) = 2.005$, $p = 0.085$, Fig. 5I). Consistent with the differences in myelin gene expression, these results suggest that EV treatment may stimulate expression of actively-myelinating, BCAS1++ expressing oligodendrocytes to promote myelin maintenance.

3.6. Relationships of oligodendroglia populations and motor recovery

Finally, we assessed whether the density and distribution of oligodendrocyte populations were correlated with the density of myelinated axons, as well as with behavioral measures of recovery (the time to recover function) based on data from Moore et al., (2019). We found the density of BCAS1++/CC1+ ($r = 0.678$, $p = 0.045$, Fig. 7A) and CC1+ ($r = 0.748$, $p = 0.021$, Fig. 7B) cells were significantly correlated with the density of myelinated axons. To further assess whether these cell populations were associated with a physiologic outcome, we compared these myelin measures with "Days to Return to Pre-Operative Latency" as described in Moore et al. (2019). Interestingly, the density of myelinated axons strongly correlated with a more rapid rate of functional recovery ($r = -0.866$, $p = 0.003$, Fig. 7C). However, there was no significant relationship between the density of BCAS1++/CC1+ cells and time to recovery ($r = -0.578$, $p = 0.103$, Fig. 7D). We hypotheisized that there was no significant relationship between denisty and recovery time because of potentially opposite correlational trends (*i.e.* positive *vs.* negative correlations) between groups. However, further correlational analyses of group-specific data did not show significant relationships between time to recovery and BCAS1++/CC1+ densities. Nevertheless, although BCAS1++/CC1+ density and recovery time were not significantly correlated, increased densities of CC1+ cells significantly correlated with reduced time to recovery ($r = -0.844$, $p = 0.004$, Fig. 7E). These results imply that increased densities of mature oligodendrocytes are related to increased densities of myelinated axons as well as reduced recovery times.

4. Discussion

4.1. Summary of results

The present study used biochemical, histological, and imaging techniques to assess changes in myelin and oligodendrocyte markers in the brain tissue and CSF of aged monkeys after cortical injury that were treated with MSC-EVs or a vehicle. The overall findings revealed that at 14 weeks after injury: (1) The density of myelinated axons is greater and are more well-organized in the EV treated group; (2) There were significantly lower densities of oligodendrocytes with oxidative DNA damage (8OHdG+) present in the EV group; (3) While MBP levels in the CSF were similar between treatment groups longitudinally, there is increased gene expression of myelin-related genes in the EV group,

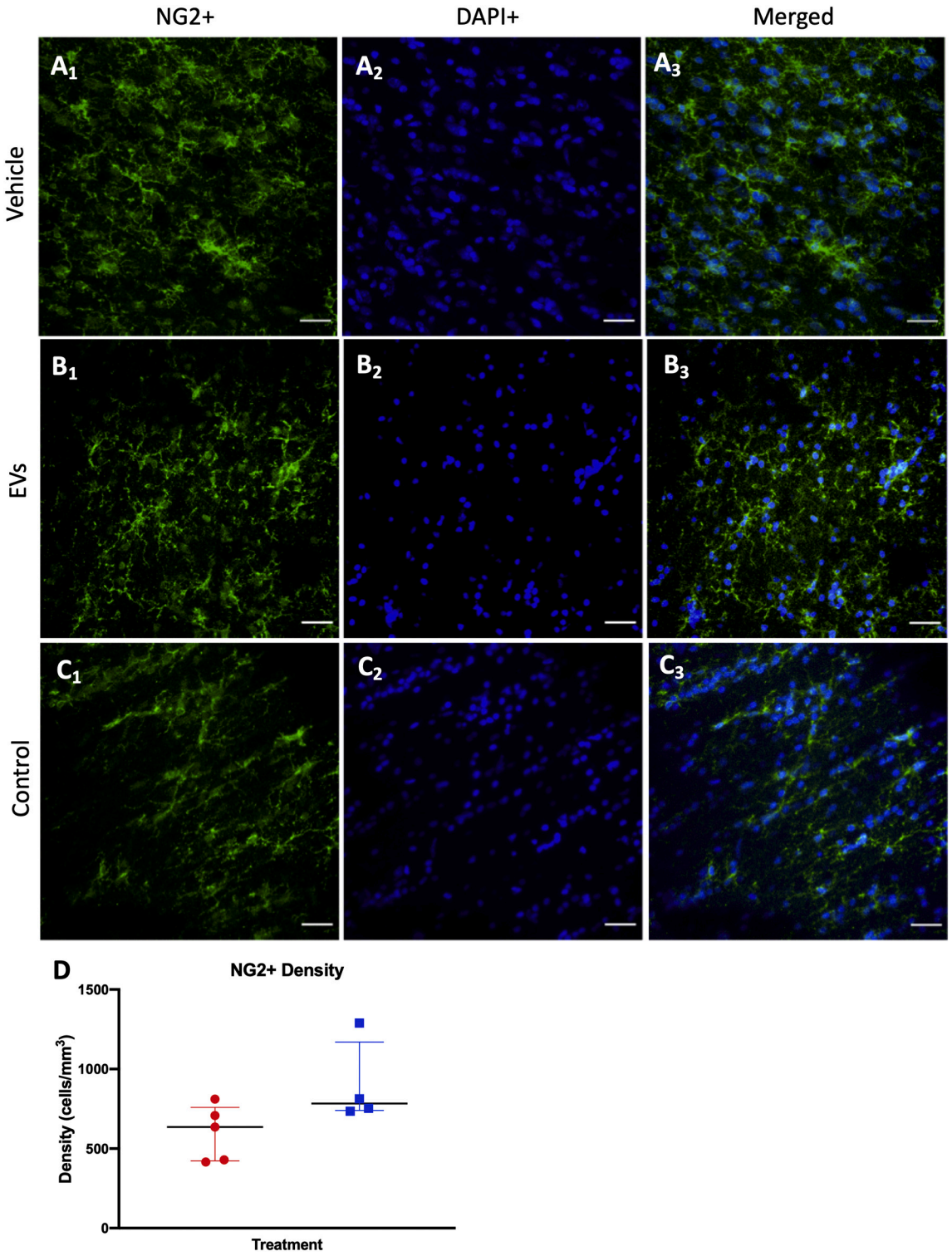

Fig. 4. Oligodendrocyte precursor cell densities are not significantly different between groups. A_1, B_1, and C_1) Confocal images of oligodendrocyte precursor cells marked by NG2. A_2, B_2, and C_2) Counterstaining of cell nuclei using DAPI. A_3, B_3, and C_3) Merged images of NG2+ labeling and DAPI counterstaining. C_1 – C_3) Representative images of NG2+ and DAPI labeling in the contralateral white matter of the motor cortex illustrates the typical distribution of NG2+ cells in an unlesioned monkey. D) Analysis of NG2+ cell densities revealed no statistically significant differences in the densities of NG2+ oligodendrocyte precursor between groups. Scale bar = 50 μm.

relative to the vehicle control group; (4) EV treatment significantly increased the density of mature CC1+ cells and new, myelinating BCAS1++/CC1-, BCAS1++/CC1+, but not immature BCAS1+/CC1- oligodendrocytes. While the BCAS1+/CC1+ cells were not significantly different between groups, there was a trend towards increased BCAS1+/CC1+ cells in the EV group; (5) The densities of BCAS1++/CC1+ and CC1+ oligodendroglia correlated with increased densities of myelinated axons as well as more rapid recovery rates. These results suggest that overall, EV treatment reduced myelin damage and enhanced myelin maintenance following cortical injury in aged brains. These changes in

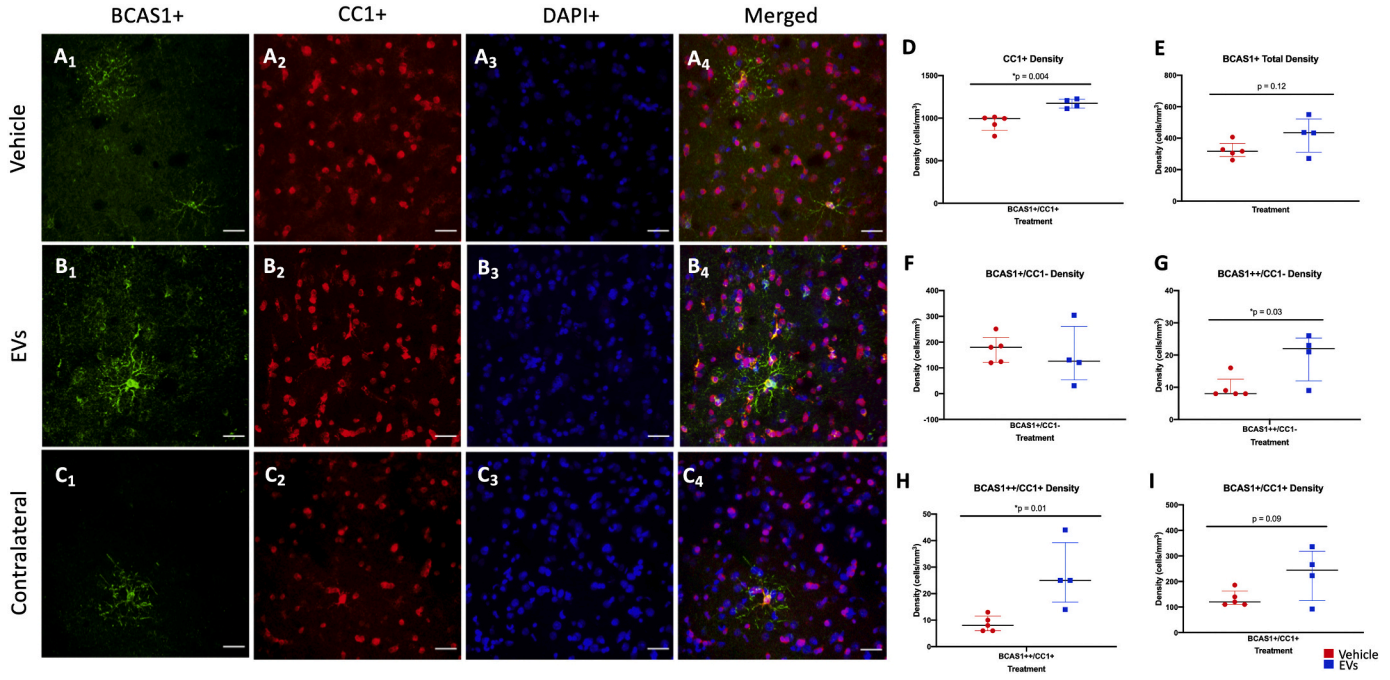

Fig. 5. Greater densities of myelinating oligodendrocytes in the EV-treated group. A_1, B_1, and C_1) Representative images of oligodendrocytes stained with BCAS1, a marker of new myelinating oligodendrocytes. A_2, B_2, and C_2) Oligodendrocytes labeled with CC1, a marker of mature, myelinating oligodendrocytes. A_3, B_3, and C_3) DAPI counterstaining was used to label cell nuclei. C_1 – C_4) Representative images of BCAS1+, CC1+, and DAPI labeling in the contralateral white matter of the motor cortex represents the typical distribution of BCAS1+ and CC1+ cells. D) There were significantly more CC1+ cell densities ($p = 0.004$) in the EV animals. E) The combined densities of all BCAS1+ cells were not different between treatment groups ($p = 0.12$). F–I) The BCAS1+ cells were further stratified into the various stages of maturation (BCAS1+/CC1-, BCAS1++/CC1-, BCAS1++/CC1+, BCAS1+/CC1+). Within these subpopulations, we found F) no statistically significant differences between groups in the BCAS1+/CC1- cells ($p = 0.67$). G) We found greater densities of BCAS1++/CC1- cells ($p = 0.03$) and H) BCAS1++/CC1+ cells ($p = 0.01$) in the EV group. I) However, the densities of BCAS1+/CC1+ cells were not different between groups ($p = 0.12$). Scale bar = 50 μm.

myelination likely contributed to EV-mediated recovery of fine motor function after cortical injury, as changes in myelination have consistently been shown to be a factor in recovery from brain injury across species (Arai and Lo 2009; Wang et al. 2016; Takase et al. 2018).

4.2. *EV treatment limits myelin damage and enhances myelin maintenance after cortical injury in the aged brain*

Oligodendrocytes are vulnerable to insults including stroke, Multiple Sclerosis, and traumatic brain injury (TBI). Damage to oligodendrocytes results in disrupted neurological function (Dewar et al. 2003; Zhang et al. 2013), so alimiting oligodendrocyte damage as well as promoting oligodendrocyte maturation to stimulate myelin maintenance are critical factors to restore neurological function after injury or disease (Miron et al. 2011; Zhang et al. 2013; Lampron et al. 2015; Shobin et al. 2017; Lloyd and Miron 2019). In the present study, we examined the brain tissue of aged monkeys treated with a novel therapeutic, MSC-EVs, which facilitated recovery of function. Specifically, we assessed whether MSC-EVs enhanced myelination after injury (Zhang and Chopp 2009; Zhang et al. 2013; Moore et al. 2019).

We first quantified the density of myelinated axons in sublesional white matter using ScoRe microscopy and found that there was a greater density of myelinated axons in the brains from EV-treated monkeys. While interesting, this did not explain whether this was a result of limiting demyelination or facilitating myelin maintenance. Thus, we performed further studies to assess EV-mediated effects on oligodendrocyte damage and maturation. The results showed that, overall, EVs acted on both processes to improve myelination. Specifically, we showed that there were lower levels of oligodendrocyte oxidative DNA damage in the EV treated group compared to the vehicle control group. Additionally, qualitative observation of oligodendrocytes showed a tendency of Olig2 localization in the nucleus in EV treated animals, while typically localizing in the cytoplasm of oligodendrocytes in the vehicle control animals. Interestingly, previous literature has shown that nuclear Olig2 localization is a characteristic of oligodendrocytes that maintain an oligodendrocytic phenotype and are found in maturing or fully mature oligodendrocytes (Setoguchi and Kondo 2004; Yokoo et al. 2004; Cassiani-Ingoni et al. 2006; Zhu et al. 2012). In contrast, Olig2 that has been exported from the nucleus into the cytoplasm, as seen in the vehicle control animals, is generally associated with cells that are more likely to switch towards astrocytic phenotypes rather than maintaining an oligodendrocytic phenotype (Setoguchi and Kondo 2004; Yokoo et al. 2004; Cassiani-Ingoni et al. 2006; Zhu et al. 2012). Hence, while Olig2+ cells in the EV group showed Olig2+ localization in the nucleus, likely indicating a stable oligodendrocytic phenotype, Olig2 immunoreactivity in the cytoplasm of the vehicle control animals suggests a shift away from the oligodendrocytic phenotypes towards an astrocytic phenotype. This further suggests that oligodendrocyte function and myelination was maintained and enhanced in the EV-treated group. Future studies are needed to further explore the potential phenotypic shift in oligodendrocyte populations between groups.

Next, at 14 weeks post-injury, we found that the EV-treated group had increased gene expressions of MyRF (regulation and differentiation of oligodendrocytes), MBP (mature oligodendrocytes), and BCAS1 (new myelinating oligodendrocytes), which are myelin-production related genes that are upregulated during myelin maintenance (Miron et al. 2011; Lloyd and Miron 2019). To further analyze oligodendrocyte maintenance, we assessed the densities of immature, maturing, and mature oligodendrocyte populations. Our data demonstrated that EV-treatment was associated with greater densities of oligodendroglia that were are associated with more mature stages of myelinating oligodendrocytes (BCAS1++/CC1+ (myelinating & mature), BCAS1++/CC1- (myelinating but not fully mature), and CC1+ (mature and stable) cells (Fard et al., 2017)). However, we found no significant differences

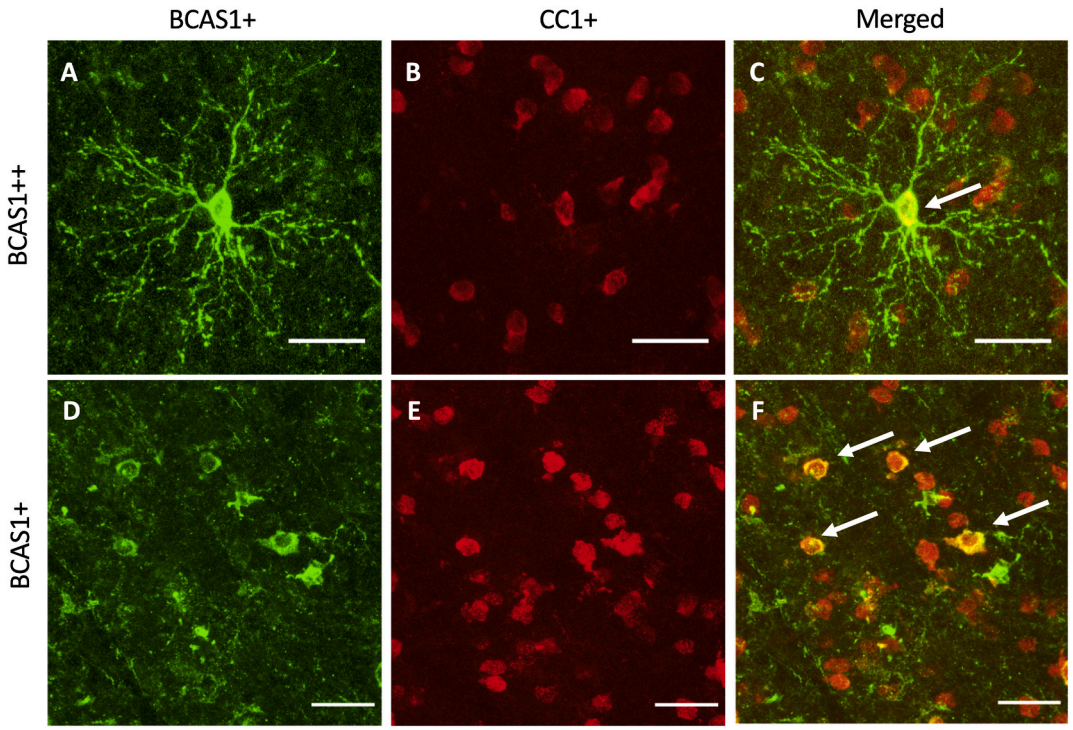

Fig. 6. BCAS1 defines a population of new myelinating oligodendrocytes. Confocal images showing cells with BCAS1 and CC1 labeling were stratified into five classes to identify oligodendrocytes at various stages of maturation: BCAS1+/CC1-, BCAS1++/CC1-, BCAS1++/CC1+, BCAS1+/CC1+, and BCAS1-/CC1+. A) High expressing BCAS1 (BCAS1++) cells were identified as cells that were immuno-reactive to BCAS1 staining both in the soma and radiating processes. B&E) CC1+ expression labeled mature, myelinating oligodendrocytes. C) A merged image of a high expressing BCAS1+ cell, with CC1+ staining. D) Low expressing BCAS1+ cells were defined by low BCAS1 immunoreactivity in the cell processes, and strong immunoreactivity constrained to the soma. F) A merged image of low expressing BCAS1+ cells with and without CC1+ co-labeling. Arrows mark cells co-labeled with BCAS1+ and CC1+ staining. Scale bar = 50 μm.

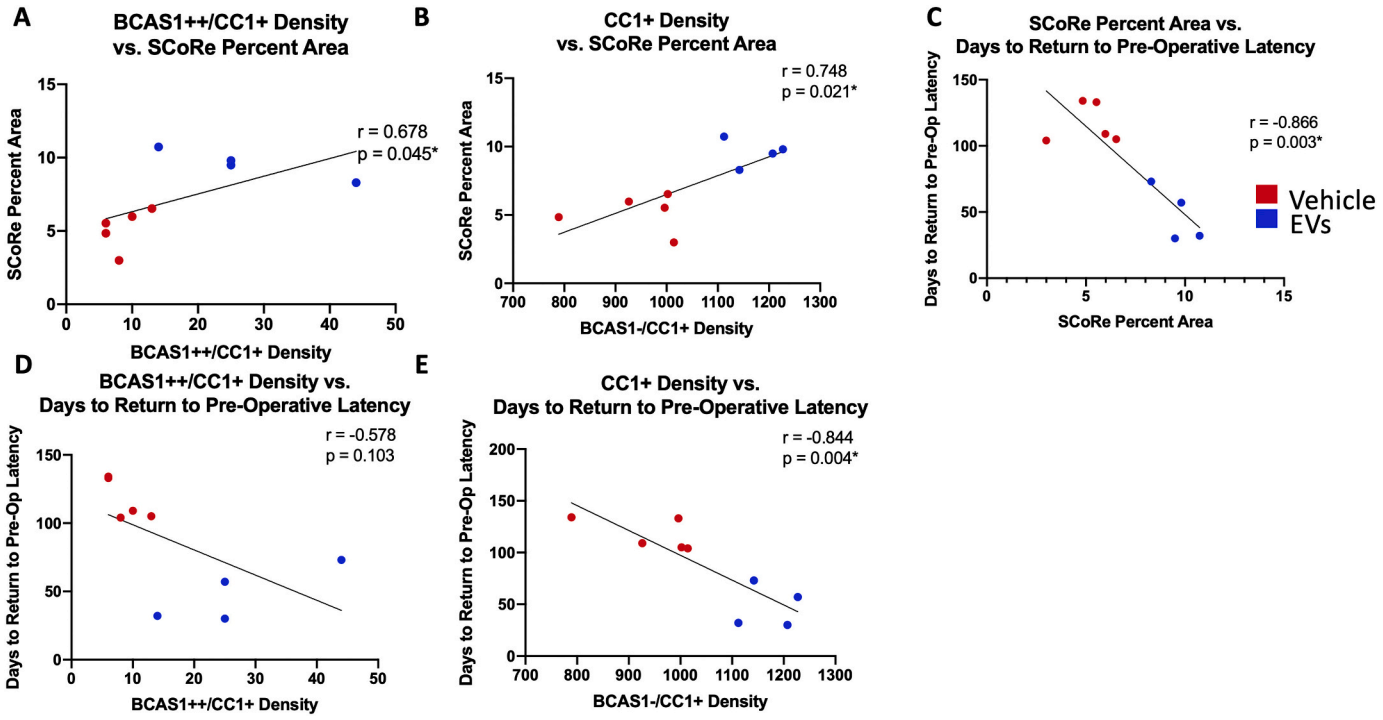

Fig. 7. Densities of myelinating oligodendrocytes correlate with the density of myelinated axons and motor recovery. A) The density of BCAS1++/CC1+ cells correlated with increased densities of myelinated axons ($p = 0.045$). B) The density of CC1+ oligodendrocytes correlated with increased densities of myelinated axons ($p = 0.021$). C) The density of myelinated axons correlated with reduced time to recovery ($p = 0.003$). D) The density of BCAS1++/CC1+ cells did not have a statistically significant relationship with time to recovery ($p = 0.103$). E) However, the density of CC1+ cells significantly correlated with reduced time to recovery ($p = 0.004$).

in the densities of NG2+ OPCs nor the immature stages of oligodendrocyte maturation (BCAS1+/CC1-) between groups.

Finally, we assessed the relationships of oligodendrocyte densities with the densities of myelinated axons (SCoRe) and measures of recovery of fine motor function of the hand (Moore et al. 2019) with and without EV treatment. We found that mature oligodendrocyte populations were correlated with greater densities of myelinated axons and reduced time to recover to baseline fine motor functions. Overall, our results suggest that EVs reduced damage to oligodendrocytes, promoted oligodendrocyte maturation to enhance myelin maintenance in aged brains, and likely underlies the enhanced motor recovery shown in Moore et al. (2019). Thus, while future experiments are needed to specifically examine the effect of EVs on oligodendrocyte maturation, our findings suggest that EV treatment specifically facilitated myelination and recovery.

4.3. Potential mechanisms and additional EV targets

In the present study, we focused on assessing changes in oligodendrocytes and myelin *in vivo*. Our data are consistent with *in vitro* studies showing that MSC-EVs promote neuronal growth and increase myelination in organotypic slice cultures, likely through the miR-17-92 cluster (Xin et al. 2017; Zhang et al. 2019), while also promoting survival, proliferation and maturation of oligodendrocytes in primary cultures (Miron et al. 2011; Kurachi et al. 2016; Osorio-Querejeta et al. 2018; Lloyd and Miron 2019). Further *in vivo* studies in rodent models of injury have shown that MSC-EVs stimulate myelination and promote oligodendrocyte survival (Ma et al. 2017). However, whether EVs act directly or indirectly on oligodendrocytes, neurons, or other glial types *in vivo* remains unknown. EVs likely act on many cell types to enhance recovery, especially since EVs contain a wide variety of miRNA, RNA, and protein (Anderson et al. 2016; Phinney and Pittenger 2017; Ferguson et al. 2018; Go et al. 2019). Because there is a plethora of molecular contents in EVs, EVs have the potential to modulate multiple cell types in the CNS, such as neurons, astrocytes, endothelial cells, microglia, and peripheral immune cells to reduce pathology and enhance recovery (Xin et al. 2012, 2013; Go et al. 2019; Zhang et al. 2019; Medalla et al. 2020). While it would be beneficial to determine the distribution of EVs within cells in our monkey model of cortical injury.

We did not perform any biodistribution analyses in the current study due to the necessity of sacrificing animals acutely after drug injection, which is a limitation of the study. However, previous *in vitro* and *in vivo* studies have shown that EVs are preferentially engulfed by endothelial cells, neurons, and glia localizing to perilesional areas after injury (Zhang et al. 2019). Thus, while it is impossible to know whether our EVs reached the site of injury to act locally, it is plausible. Additionally, while EVs can act directly on CNS cells, they can also act indirectly by modulating cells to perform different biological functions and influence neighboring cells (Zhang et al. 2019). For instance, it is possible that changes in microglial reactivity could influence surrounding cells (Go et al. 2019). Specifically, microglial shifts from damaging, reactive phenotypes towards surveilling phenotypes could increase the release of growth factors and anti-inflammatory cytokines to promote regeneration and neurorestoration after injury (Patel et al. 2013; Go et al. 2019). Additionally, it is now known that myelin dynamics are often influenced by the activity of neurons (de Faria et al. 2019). Indeed, our previous work has specifically shown that EV treatment reduced microgliosis (Go et al. 2019), and neuronal pathology (Medalla et al. 2020). Therefore, while we show here that EVs clearly modulate myelination after cortical injury, it is unclear whether the changes in oligodendrocytes and myelin maintenance was a direct or indirect effect of EV therapy. It is likely that the effects of EVs on each of these cell populations and the interactions between the cells targeted have a combined effect on motor recovery in our monkey model of cortical injury, which may not be possible to disentangle. For example, while we showed that oxidative DNA damage was reduced in the oligodendrocytes of EV-treated monkeys, additional modes of damage to oligodendrocytes, such as degrading enzymes or pro-inflammatory cytokines, may have also contributed to oligodendrocyte damage (Sloane et al. 2003; Chavez et al. 2009; Tse and Herrup 2017). Thus, while this report has focused on changes in oligodendrocytes, EV treatment likely modulated many cell types, both directly and indirectly, to improve recovery. Finally, while previous proteomic and transcriptomic studies have characterized the contents of human, porcine, and rodent MSC-EVs, (Anderson et al. 2016; Eirin et al. 2016; Ferguson et al. 2018; van Balkom et al., 2019), the constituents of the monkey MSC-EVs used here have not been characterized. Future work is geared towards large scale proteomic and transcriptomic analyses to identify the active components in these monkey EVs, as well as using *in vitro* models to tease apart the precise molecular pathways and cellular targets modulated by EV-treatment.

4.4. Implications for the aged brain and white matter pathologies

The efficacy of EVs in enhancing oligodendrocyte and myelin maintenance after cortical injury shown here is consistent with the use of EVs as treatment for other brain pathologies where white matter is affected, such as Multiple Sclerosis, Spinal Cord Injury, Chronic Traumatic Encephalopathy, and aging (Xin et al. 2012; Rani et al. 2015; Williams et al. 2019). Most relevant to the current study is the growing evidence of the efficacy of MSC-EVs as a possible intervention in aging (Panagiotou et al. 2018). Normal brain aging is characterized by chronic myelin pathology and oligodendrocyte dysfunction, which are strongly correlated with age-related cognitive decline (Bowley et al. 2010; Schain et al. 2014; de Lange et al. 2016). Further, there is evidence showing that this age-related white matter damage is linked to chronic inflammation (Duce et al. 2006; Shobin et al. 2017). The accumulation of myelin damage, inflammation, and oxidative stress in the aged brain underlies its increased susceptibility to ischemic brain injury (Crack and Taylor 2005; Gemma et al. 2007; Shobin et al. 2017), but also represents specific candidate targets for interventions (Cornejo and von Bernhardi, 2016; Robillard et al., 2016; Safaiyan et al., 2016; Xie et al., 2013).

Previous work in monkeys from our laboratory has shown age-related increases in myelin damage (Peters 2002; Bowley et al. 2010) and microglial activation (Shobin et al. 2017) associated with cognitive decline in aged monkeys. This is of particular interest to the present study, as the brain tissue and CSF came from monkeys within the age range in which we begin to see myelin atrophy, white matter degeneration, and cognitive decline (Shobin et al. 2017). The comprehensive findings in this study show that EVs reduce myelin damage and enhance myelin maintenance following cortical injury in aged brains. Overall, these findings provide rationale for testing MSC-EVs for white matter pathologies associated not only acquired neurological injuries or degenerative diseases, but also with normal aging.

4.5. Future directions and limitations

One limitation of the study is that the temporal sequence of MSC-EV action on oligodendrocytes cannot be addressed given the current cross-sectional model with brain tissue harvested at 14 weeks after injury. Therefore, future studies are needed to examine brain tissue at earlier timepoints to assess myelination across the recovery period. While it would be ideal to assess tissue across the entirety of the recovery period, including at 24 h after injury, the feasibility of these experiments is challenging due to the high cost of monkeys and resources necessary to complete these studies. Additionally, our sample size was small and was limited only to female subjects. An increased sample size including both sexes will be needed in the future to not only confirm some of the trends observed in this study, but to also address potential sex-related effects. An increase in sample size will also allow within-group correlation analyses that may reveal treatment-specific relationships of myelination and recovery. An additional caveat with this study is the use of a single donor of MSC-EVs. While the therapeutic effects of EVs from multiple

donors will be important to study in the future, the use of a single donor in this study limited the variability that could arise from using EVs from various donors. Furthermore, future work using novel monkey and human *in vitro* culture and organoid systems will be important to characterize the precise molecular pathways and the mechanisms of action of MSC-EVs on oligodendrocytes and other cell types. Thus, while we show the therapeutic benefits of EVs on myelination and functional recovery in our aged monkey model of cortical injury *in vivo*, additional studies are needed to further characterize the mechanisms that underlie the full therapeutic potential of MSC-EVs.

5. Conclusions

This study provides novel evidence in aged rhesus monkeys supporting the hypothesis that MSC-EVs act on oligodendrocytes to facilitate recovery of function. Specifically, we show that EV treatment likely did this in part by limiting damage to oligodendrocyte DNA and by enhancing myelin maintenance through upregulating myelin-related gene expression and increasing the population of actively-myelinating oligodendrocytes. While these results emphasize the importance of oligodendroglia and myelin, it is likely that MSC-EVs also modified other cells to enhance recovery of function. Thus, while our results explain some of the cellular changes that enhanced recovery, they likely only partially explain the cellular and molecular changes that occurred with EV-treatment to enhance overall recovery after cortical injury.

Funding

This work was supported by NIH grants R21-NS102991, R21-NS111174, and U01-NS076474 as well as through BU-CTSI Grant Number 1UL1TR001430 through the National Center for Advancing Translational Sciences at the National Institutes of Health.

Declaration of Competing Interests

The authors report no competing interests.

Acknowledgements

We would like to acknowledge our colleagues, Penny Schultz, Karen Slater, Karen Bottenfield, Katelyn Trecartin, Samantha Calderazzo, and Ajay Uprety for their valuable assistance with this study. We would also like to thank Cidi Chen for allowing us to use the ELISA plate reader, as well as the Whitaker Cardiovascular Institute for allowing us to use their PCR equipment.

Appendix A. Supplementary data

Supplementary data to this article can be found online at https://doi.org/10.1016/j.expneurol.2020.113540.

References

Orczykowski, M., Calderazzo, Samantha M., Shobin, Eli, Pessina, Monica A., Oblak, Adrian L., Finklestein, Seth P., Kramer, B.C., Mortazavi, Farzad, Rosene, Douglas L., Moore, Tara L., 2018. Cell Based Therapy Mediates Immunomodulation and reduction of Secondary Damage Following Cortical Injury (Manuscript in preparation).

Alizadeh, A., Dyck, S.M., Karimi-Abdolrezaee, S., 2015. Myelin damage and repair in pathologic CNS: challenges and prospects. Front. Mol. Neurosci. 8. Available at: https://www.ncbi.nlm.nih.gov/pmc/articles/PMC4515562/. (Accessed 19 September 2019).

Anderson, J.D., et al., 2016. Comprehensive proteomic analysis of mesenchymal stem cell exosomes reveals modulation of angiogenesis via nuclear factor-KappaB signaling. Stem Cells 34, 601–613.

Arai, K., Lo, E.H., 2009. Experimental models for analysis of oligodendrocyte pathophysiology in stroke. Exp. Trans. Stroke Med. 1, 6.

van Balkom, B.W.M., Gremmels, H., Giebel, B., Lim, S.K., 2019. Proteomic signature of mesenchymal stromal cell-derived small extracellular vesicles. PROTEOMICS 19, 1800163.

Bowley, M.P., Cabral, H., Rosene, D.L., Peters, A., 2010. Age changes in myelinated nerve fibers of the cingulate bundle and corpus callosum in the rhesus monkey. J. Comp. Neurol. 518, 3046–3064.

Cassiani-Ingoni, R., Coksaygan, T., Xue, H., Reichert-Scrivner, S.A., Wiendl, H., Rao, M. S., Magnus, T., 2006. Cytoplasmic translocation of Olig2 in adult glial progenitors marks the generation of reactive astrocytes following autoimmune inflammation. Exp. Neurol. 201, 349–358.

Chavez, J.C., Hurko, O., Barone, F.C., Feuerstein, G.Z., 2009. Pharmacologic interventions for stroke: looking beyond the thrombolysis time window into the penumbra with biomarkers, not a stopwatch. Stroke 40, e558–e563.

Chopp, M., Li, Y., 2002. Treatment of neural injury with marrow stromal cells. Lancet Neurol. 1, 92–100.

Cornejo, F., von Bernhardi, R., 2016. Age-Dependent Changes in the Activation and Regulation of Microglia. Adv. Exp. Med. Biol. 949, 205–226. https://doi.org/10.1007/978-3-319-40764-7_10. PMID: 27714691.

Crack, P.J., Taylor, J.M., 2005. Reactive oxygen species and the modulation of stroke. Free Radic. Biol. Med. 38, 1433–1444.

Dewar, D., Yam, P., McCulloch, J., 1999. Drug development for stroke: importance of protecting cerebral white matter. Eur. J. Pharmacol. 375, 41–50.

Dewar, D., Underhill, S.M., Goldberg, M.P., 2003. Oligodendrocytes and ischemic brain injury. J. Cereb. Blood Flow Metab. 23, 263–274.

Duce, J.A., Hollander, W., Jaffe, R., Abraham, C.R., 2006. Activation of early components of complement targets myelin and oligodendrocytes in the aged rhesus monkey brain. Neurobiol. Aging 27, 633–644.

Duncan, I.D., Grever, W.E., Zhang, S.-C., 1997. Repair of myelin disease: strategies and progress in animal models. Mol. Med. Today 3, 554–561.

Eirin, A., Zhu, X.-Y., Puranik, A.S., Woollard, J.R., Tang, H., Dasari, S., Lerman, A., van Wijnen, A.J., Lerman, L.O., 2016. Comparative proteomic analysis of extracellular vesicles isolated from porcine adipose tissue-derived mesenchymal stem/stromal cells. Sci. Rep. 6, 36120.

El Waly, B., Macchi, M., Cayre, M., Durbec, P., 2014. Oligodendrogenesis in the normal and pathological central nervous system. Front. Neurosci. 8. Available at: https://www.ncbi.nlm.nih.gov/pmc/articles/PMC4054666/ [Accessed October 24, 2019].

Fard, M.K., van der Meer, F., Sánchez, P., Cantuti-Castelvetri, L., Mandad, S., Jäkel, S., Fornasiero, E.F., Schmitt, S., Ehrlich, M., Starost, L., Kuhlmann, T., Sergiou, C., Schultz, V., Wrzos, C., Brück, W., Urlaub, H., Dimou, L., Stadelmann, C., Simons, M., 2017. BCAS1 expression defines a population of early myelinating oligodendrocytes in multiple sclerosis lesions. Sci. Transl. Med. 9, eaam7816.

de Faria, O., Gonsalvez, D.G., Nicholson, M., Xiao, J., 2019. Activity-dependent central nervous system myelination throughout life. J. Neurochem. 148, 447–461.

Ferguson, S.W., Wang, J., Lee, C.J., Liu, M., Neelamegham, S., Canty, J.M., Nguyen, J., 2018. The microRNA regulatory landscape of MSC-derived exosomes: a systems view. Sci. Rep. 8, 1419.

Fiala, J.C., Harris, K.M., 2001. Extending unbiased stereology of brain ultrastructure to three-dimensional volumes. J. Am. Med. Inform. Assoc. 8, 1–16.

Gemma, C., Vila, J., Bachstetter, A., Bickford, P.C., 2007. Oxidative stress and the aging brain: from theory to prevention. In: Brain aging: Models, Methods, and Mechanisms. CRC Press, Boca Raton, FL, US, pp. 353–374. Frontiers in neuroscience.

Go, V., Bowley, B.G.E., Pessina, M.A., Zhang, Z.G., Chopp, M., Finklestein, S.P., Rosene, D.L., Medalla, M., Buller, B., Moore, T.L., 2019. Extracellular vesicles from mesenchymal stem cells reduce microglial-mediated neuroinflammation after cortical injury in aged rhesus monkeys. GeroSci. 42 (1-17) https://doi.org/10.1007/s11357-019-00115-w. Available at: [Accessed November 6, 2019].

Hill, R.A., Li, A.M., Grutzendler, J., 2018. Lifelong cortical myelin plasticity and age-related degeneration in the live mammalian brain. Nat. Neurosci. 21, 683–695.

Kurachi, M., Mikuni, M., Ishizaki, Y., 2016. Extracellular vesicles from vascular endothelial cells promote survival, proliferation and motility of oligodendrocyte precursor Cells. PLoS One 11. Available at: https://www.ncbi.nlm.nih.gov/pmc/articles/PMC4942096/. (Accessed 25 April 2020).

Lakhan, S.E., Kirchgessner, A., Hofer, M., 2009. Inflammatory mechanisms in ischemic stroke: therapeutic approaches. J. Transl. Med. 7, 97.

Lampron, A., Larochelle, A., Laflamme, N., Préfontaine, P., Plante, M.-M., Sánchez, M.G., Yong, V.W., Stys, P.K., Tremblay, M.-È., Rivest, S., 2015. Inefficient clearance of myelin debris by microglia impairs remyelinating processes. J. Exp. Med. 212, 481–495.

de Lange, A.-M.G., Bråthen, A.C.S., Grydeland, H., Sexton, C., Johansen-Berg, H., Andersson, J.L.R., Rohani, D.A., Nyberg, L., Fjell, A.M., Walhovd, K.B., 2016. White matter integrity as a marker for cognitive plasticity in aging. Neurobiol. Aging 47, 74–82.

Lloyd, A.F., Miron, V.E., 2019. The pro-remyelination properties of microglia in the central nervous system. Nat. Rev. Neurol. 15, 447–458.

Ma, Y., Ge, S., Zhang, J., Zhou, D., Li, L., Wang, X., Su, J., 2017. Mesenchymal stem cell-derived extracellular vesicles promote nerve regeneration after sciatic nerve crush injury in rats. Int. J. Clin. Exp. Pathol. 10, 10032–10039.

Medalla, M., Luebke, J.I., 2015. Diversity of glutamatergic synaptic strength in lateral prefrontal versus primary visual cortices in the rhesus monkey. J. Neurosci. 35, 112–127.

Medalla, M., Chang, W., Calderazzo, S.M., Go, V., Tsolias, A., Goodliffe, J.W., Pathak, D., Alba, D.D., Pessina, M., Rosene, D.L., Buller, B., Moore, T.L., 2020. Treatment with mesenchymal-derived extracellular vesicles reduces injury-related pathology in pyramidal neurons of monkey perilesional ventral premotor cortex EVs reduce injury-related pathology in vPMC. J. Neurosci. 40 (17), 3385–3407. https://doi.org/10.1523/JNEUROSCI.2226-19.2020. Epub 2020 Apr 2. PMID: 32241837; PMCID: PMC7178914 Available at: https://www.jneurosci.org/content/early/2020/03/27/JNEUROSCI.2226-19.2020. (Accessed 16 April 2020).

Michel, K., Zhao, T., Karl, M., Lewis, K., Fyffe-Maricich, S.L., 2015. Translational control of myelin basic protein expression by ERK2 MAP kinase regulates timely remyelination in the adult brain. J. Neurosci. 35, 7850–7865.
Miron, V.E., Kuhlmann, T., Antel, J.P., 2011. Cells of the oligodendroglial lineage, myelination, and remyelination. Biochim. Biophys. Acta 1812, 184–193.
Miyamoto, N., Pham, L.-D.D., Hayakawa, K., Matsuzaki, T., Seo, J.H., Magnain, C., Ayata, C., Kim, K.-W., Boas, D., Lo, E.H., Arai, K., 2013. Age-related decline in oligodendrogenesis retards white matter repair in mice. Stroke 44, 2573–2578.
Moore, T.L., Killiany, R.J., Pessina, M.A., Moss, M.B., Finklestein, S.P., Rosene, D.L., 2012. Recovery from ischemia in the middle-aged brain: a nonhuman primate model. Neurobiol. Aging 33, 619.e9-619.e24.
Moore, T.L., Pessina, M.A., Finklestein, S.P., Kramer, B.C., Killiany, R.J., Rosene, D.L., 2013. Recovery of fine motor performance after ischemic damage to motor cortex is facilitated by cell therapy in the rhesus monkey. Somatosens. Mot. Res. 30, 185–196.
Moore, T.L., Bowley, B.G.E., Pessina, M.A., Calderazzo, S.M., Medalla, M., Go, V., Zhang, Z.G., Chopp, M., Finklestein, S., Harbaugh, A.G., Rosene, D.L., Buller, B., 2019. Mesenchymal derived exosomes enhance recovery of motor function in a monkey model of cortical injury. Restor. Neurol. Neurosci. 37, 347–362.
Ohta, M., Ohta, K., 2002. Detection of myelin basic protein in cerebrospinal fluid. Expert. Rev. Mol. Diagn. 2, 627–633.
Osorio-Querejeta, I., Alberro, A., Muñoz-Culla, M., Mäger, I., Otaegui, D., 2018. Therapeutic potential of extracellular vesicles for demyelinating diseases; challenges and opportunities. Front. Mol. Neurosci. 11. Available at: https://www.ncbi.nlm.nih.gov/pmc/articles/PMC6265410/. (Accessed 7 September 2020).
Panagiotou, M., Papagiannopoulos, K., Rohling, J.H.T., Meijer, J.H., Deboer, T., 2018. How old is your brain? Slow-Wave Activity in Non-rapid-eye-movement Sleep as a Marker of Brain Rejuvenation After Long-Term Exercise in Mice. Front. Aging Neurosci. 10. Available at: https://www.frontiersin.org/articles/10.3389/fnagi.2018.00233/full [Accessed April 24, 2020].
Patel, A.R., Ritzel, R., McCullough, L.D., Liu, F., 2013. Microglia and ischemic stroke: a double-edged sword. Int. Journal . Physiol. Pathophysiol. Pharmacol. 5, 73–90.
Peters, A., 2002. The effects of normal aging on myelin and nerve fibers: a review. J. Neurocytol. 31, 581–593.
Phinney, D.G., Pittenger, M.F., 2017. Concise review: MSC-derived exosomes for cell-free therapy. Stem Cells 35, 851–858.
Rani, S., Ryan, A.E., Griffin, M.D., Ritter, T., 2015. Mesenchymal stem cell-derived extracellular vesicles: toward cell-free therapeutic applications. Mol. Ther. 23, 812–823.
Rivera, A., Vanzuli, I., Arellano, J.J.R., Butt, A., 2016. Decreased regenerative capacity of oligodendrocyte progenitor cells (NG2-glia) in the ageing brain: a vicious cycle of synaptic dysfunction, myelin loss and neuronal disruption? Curr. Alzheimer Res. 13, 413–418.
Robillard, K.N., Lee, K.M., Chiu, K.B., Maclean, A.G., 2016. Glial cell morphological and density changes through the lifespan of rhesus macaques. Brain, Behavior, and Immunity 55, 60–69. https://doi.org/10.1016/j.bbi.2016.01.006.
Rosene, D.L., Roy, N.J., Davis, B.J., 1986. A cryoprotection method that facilitates cutting frozen sections of whole monkey brains for histological and histochemical processing without freezing artifact. J. Histochem. Cytochem. 34 (10), 1301–1315. https://doi.org/10.1177/34.10.3745909. Oct, PMID: 3745909.
Safaiyan, S., Kannaiyan, N., Snaidero, N., Brioschi, S., Biber, K., Yona, S., Edinger, A.L., Jung, S., Rossner, M.J., Simons, M., 2016. Age-related myelin degradation burdens the clearance function of microglia during aging. Nat Neurosci. 19 (8), 995–998. https://doi.org/10.1038/nn.4325. Aug, Epub 2016 Jun 13. PMID: 27294511.
Schain, A.J., Hill, R.A., Grutzendler, J., 2014. Label-free *in vivo* imaging of myelinated axons in health and disease with spectral confocal reflectance microscopy. Nat. Med. 20, 443–449.
Schnell, S.A., Staines, W.A., Wessendorf, M.W., 1999. Reduction of lipofuscin-like autofluorescence in fluorescently labeled tissue. J. Histochem. Cytochem. 47, 719–730.
Setoguchi, T., Kondo, T., 2004. Nuclear export of OLIG2 in neural stem cells is essential for ciliary neurotrophic factor–induced astrocyte differentiation. J. Cell Biol. 166, 963–968.
Shobin, E., Bowley, M.P., Estrada, L.I., Heyworth, N.C., Orczykowski, M.E., Eldridge, S. A., Calderazzo, S.M., Mortazavi, F., Moore, T.L., Rosene, D.L., 2017. Microglia activation and phagocytosis: relationship with aging and cognitive impairment in the rhesus monkey. GeroScience 39, 199–220.
Sloane, J.A., Hinman, J.D., Lubonia, M., Hollander, W., Abraham, C.R., 2003. Age-dependent myelin degeneration and proteolysis of oligodendrocyte proteins is associated with the activation of calpain-1 in the rhesus monkey. J. Neurochem. 84, 157–168.
Sozmen, E.G., Hinman, J.D., Carmichael, S.T., 2012. Models that matter: white matter stroke models. Neurotherapeutics 9, 349–358.
Takase, H., Washida, K., Hayakawa, K., Arai, K., Wang, X., Lo, E.H., Lok, J., 2018. Oligodendrogenesis after traumatic brain injury. Behav. Brain Res. 340, 205–211.
Tigges, J., Gordon, T.P., McClure, H.M., Hall, E.C., Peters, A., 1988. Survival rate and life span of rhesus monkeys at the Yerkes regional primate research center. Am. J. Primatol. 15, 263–273. https://doi.org/10.1002/ajp.1350150308.
Tse, K.-H., Herrup, K., 2017. DNA damage in the oligodendrocyte lineage and its role in brain aging. Mech. Ageing Dev. 161, 37–50.
Wang, Q., Tang, X.N., Yenari, M.A., 2007. The inflammatory response in stroke. J. Neuroimmunol. 184, 53–68.
Wang, Y., Liu, G., Hong, D., Chen, F., Ji, X., Cao, G., 2016. White matter injury in ischemic stroke. Prog. Neurobiol. 141, 45–60.
Williams, A.M., Dennahy, I.S., Bhatti, U.F., Halaweish, I., Xiong, Y., Chang, P., Nikolian, V.C., Chtraklin, K., Brown, J., Zhang, Y., Zhang, Z.G., Chopp, M., Buller, B., Alam, H.B., 2019. Mesenchymal stem cell-derived exosomes provide neuroprotection and improve long-term neurologic outcomes in a swine model of traumatic brain injury and hemorrhagic shock. J. Neurotrauma 36, 54–60.
Witwer, K.W., et al., 2017. Updating the MISEV minimal requirements for extracellular vesicle studies: building bridges to reproducibility. J. Extracell. Ves. 6, 1396823.
Xie, F., Zhang, J., Fu, H., Chen, J., 2013. Age-related decline of myelin proteins is highly correlated with activation of astrocytes and microglia in the rat CNS. Int. J. Mol. Med. 32, 1021–1028. https://doi.org/10.3892/ijmm.2013.1486.
Xin, H., Li, Y., Buller, B., Katakowski, M., Zhang, Y., Wang, X., Shang, X., Zhang, Z.G., Chopp, M., 2012. Exosome-mediated transfer of miR-133b from multipotent mesenchymal stromal cells to neural cells contributes to neurite outgrowth. Stem Cells 30, 1556–1564.
Xin, H., Li, Y., Cui, Y., Yang, J.J., Zhang, Z.G., Chopp, M., 2013. Systemic administration of exosomes released from mesenchymal stromal cells promote functional recovery and neurovascular plasticity after stroke in rats. J. Cereb. Blood Flow Metab. 33, 1711–1715.
Xin, H., Katakowski, M., Wang, F., Qian, J.-Y., Shuang Liu, X., Ali, M.M., Buller, B., Zhang, Z.G., Chopp, M., 2017. MiR-17-92 cluster in exosomes enhance neuroplasticity and functional recovery after stroke in rats. Stroke 48, 747–753.
Yokoo, H., Nobusawa, S., Takebayashi, H., Ikenaka, K., Isoda, K., Kamiya, M., Sasaki, A., Hirato, J., Nakazato, Y., 2004. Anti-human Olig2 antibody as a useful immunohistochemical marker of normal oligodendrocytes and gliomas. Am. J. Pathol. 164, 1717–1725.
Zhang, Z.G., Chopp, M., 2009. Neurorestorative therapies for stroke: underlying mechanisms and translation to the clinic. Lancet Neurol. 8, 491–500.
Zhang, R., Chopp, M., Zhang, Z.G., 2013. Oligodendrogenesis after cerebral ischemia. Front. Cell. Neurosci. 7. Available at: https://www.frontiersin.org/articles/10.3389/fncel.2013.00201/full [Accessed September 19, 2019].
Zhang, Y., Chopp, M., Meng, Y., Katakowski, M., Xin, H., Mahmood, A., Xiong, Y., 2015. Effect of exosomes derived from multipluripotent mesenchymal stromal cells on functional recovery and neurovascular plasticity in rats after traumatic brain injury. J. Neurosurg. 122, 856–867.
Zhang, Z.G., Buller, B., Chopp, M., 2019. Exosomes — beyond stem cells for restorative therapy in stroke and neurological injury. Nat. Rev. Neurol. 15, 193–203.
Zhu, X., Zuo, H., Maher, B.J., Serwanski, D.R., LoTurco, J.J., Lu, Q.R., Nishiyama, A., 2012. Olig2-dependent developmental fate switch of NG2 cells. Development 139, 2299–2307.